CrystEngComm

RSC Publishing

PAPER

View Article Online
View Journal | View Issue

Cite this: *CrystEngComm*, 2013, **15**, 5434

Combinatorial substrate epitaxy: a new approach to growth of complex metastable compounds†

Sarthak Havelia, Shanling Wang,‡ K. R. Balasubramaniam,§ Andrew M. Schultz, Gregory S. Rohrer and Paul A. Salvador*

Received 15th March 2013,
Accepted 21st May 2013

DOI: 10.1039/c3ce40469b

www.rsc.org/crystengcomm

A high-throughput processing-characterization method, called combinatorial substrate epitaxy (CSE), was developed that enables the investigation of epitaxial stabilization of metastable compositions in complex structures. To demonstrate the approach, we fabricated $RE_2Ti_2O_7$ (RE = Dy, Gd, Sm, La) in a polymorphic structure for which RE = Dy, Gd, and Sm are metastable and $Dy_2Ti_2O_7$ has not been previously observed. Dense sintered pellets of $Sr_2Nb_2O_7$, which adopts the 110-layered perovskite (LP) structure, were prepared as substrates, polished flat, and characterized locally using electron backscatter diffraction (EBSD). Thin films of $RE_2Ti_2O_7$ were deposited using pulsed laser deposition and were then characterized with EBSD. The EBSD patterns from all film–substrate pairs matched in a grain-by-grain fashion, which demonstrates that the films are in local epitaxial registry with the $Sr_2Nb_2O_7$ grains over a wide spread of crystallographic orientations for the substrate surface. Furthermore, the EBSD patterns demonstrate that all $RE_2Ti_2O_7$ films, whether stable or metastable in the bulk, adopt the 110-LP structure. Transmission electron microscopy was used to investigate more closely the metastable $Sm_2Ti_2O_7$ films. The film–substrate interfaces are atomically smooth with relaxed epitaxial registry, indicating that the microcrystalline substrates can be treated as local single-crystal substrates and the metastable films are stable against back-transformation on strain relaxation. Electron diffraction patterns for $Sm_2Ti_2O_7$ films are consistent with the monoclinic 110-LP unit cells. This work demonstrates that CSE allows for the growth of new materials that are thermodynamically and kinetically difficult to realize otherwise.

1 Introduction

Epitaxial stabilization of metastable films on single crystals has greatly increased the number of compositions that form in specific crystal structures and has improved the understanding of composition–structure–property relationships in materials.[1–4] Nevertheless, the scope of structural families that have been investigated is generally limited to those, such as perovskite,[1–9] that meet two criteria: they have simple isotropic structures for which kinetic barriers to crystallization are low and they form coherent interfaces with commercially available single crystals.[10] Unfortunately, many interesting structural families do not fit these criteria, especially those having complex layered structures.[11–13] Such constraints limit the crystalline quality and the ability to form metastable phases of complex crystal structures, including Ruddlesden–Popper phases,[14] layered copper oxide superconductors,[15–21] hexagonal $AMnO_3$ compounds,[2,22–28] and 110-layered perovskite (LP) $A_2B_2O_7$ ferroelectrics,[10,29–33] among many others. One can improve the film quality and favor metastable phases by depositing on home-grown single crystal substrates that are isostructural to the targeted complex phases,[28] but single-crystal substrate preparation is onerous. In this contribution, we demonstrate a high-throughput approach that expands and generalizes epitaxial crystal engineering to complex crystal systems for which dense sintered pellets are easily fabricated.

Polycrystalline substrates are widely used for industrial coatings,[34] but rarely used in epitaxial stabilization studies. Yet, they provide a large spread of surface orientations in a single experiment, and offer a high throughput method to study the role of orientation on film growth.[35] We call this high-throughput method combinatorial substrate epitaxy (CSE),[35] a combinatorial synthesis method in which a large number of template combinations are used to stabilize a precise composition in a specific structure. This contrasts compositional spread combinatorial thin film methods,[36] which use a large number of compositions to search for new structures or properties. To carry out a CSE study, one needs both a substrate with appropriate surfaces and a robust local

Department of Materials Science and Engineering, Carnegie Mellon University, 5000 Forbes Ave, Pittsburgh, Pennsylvania, 15213, USA. E-mail: paulsalvador@cmu.edu; Tel: +1-412-268-2702

† Electronic supplementary information (ESI) available: EBSD patterns from $Sr_2Nb_2O_7$ substrates, $La_2Ti_2O_7$ films, and $Gd_2Ti_2O_7$ films, as well as HREM of a $Sm_2Ti_2O_7/Sr_2Nb_2O_7$ interface. See DOI: 10.1039/c3ce40469b

‡ Present address: Sichuan University, Analytical and Testing Center, Chengdu, 610064, P. R. China.

§ Present address: Department of Energy Science and Engineering, IIT Bombay, Mumbai, 400076, India.

structural characterization method. Electron backscatter diffraction (EBSD) is an appropriate characterization tool, having been developed over the course of the last few decades for the complete quantification of crystallographic distributions in polycrystalline microstructures.[37–40] EBSD has been used for film characterization,[41–47] though less commonly than for bulk specimens, and has been sparsely used for epitaxial film growth.[21,48–52] We recently demonstrated using CSE that the phase and orientation relationship of TiO_2 films on $BaTiO_3$[51] and $BiFeO_3$[35] polycrystals could be probed over a spread of orientation space using just one polycrystalline substrate.

CSE holds promise as an effective method for crystal engineering of complex layered phases; we focus here on the growth of metastable $A_2B_2O_7$ 110-LP compounds. Compounds in the $A_2B_2O_7$ 110-LP family are high-temperature ferroelectrics and have good photochemical activity.[13,53] Only a modest number compositions form in the closely related structural families,[13,53,54] with AE_2 $(Nb,Ta)_2O_7$ and $RE_2Ti_2O_7$ (AE, RE = alkaline earth, rare earth) being the most numerous. In the titanates, the stable 110-LP phases include RE = Nd–La;[55,56] the remaining $RE_2Ti_2O_7$ compounds adopt the pyrochlore structure.[13,53,54,57] We recently showed that (001)-oriented $RE_2Ti_2O_7$ (RE = Gd, Sm, Nd, and La) compounds could be synthesized in the 110-LP structure as films on $SrTiO_3$ (110) substrates.[58] (Several of these same phases were previously prepared using high-pressure[59] or soft-chemical methods.[60,61]) It was also found that a new kinetically preferred polymorph (called the γ phase) competes in stability with both the pyrochlore and the (001)-oriented 110-LP structure when compounds are prepared as epitaxial thin films (on several different single crystal substrates).[10] Clearly, this observation complicates crystal engineering efforts of metastable 110-LP compounds (such as for RE = Y and Dy).[10]

In this contribution, we synthesized $RE_2Ti_2O_7$ (RE = Dy, Gd, Sm, and La) compounds in the 110-LP structure using local (grain-by-grain) epitaxial stabilization on $Sr_2Nb_2O_7$ surfaces of many different crystallographic orientations, which are present on the polished sintered ceramic substrates. The results demonstrate that the 110-LP structure is preferred during epitaxial growth on 110-LP substrates; $Dy_2Ti_2O_7$ has not been fabricated in this structure previously. That the 110-LP structure can successfully compete with both the pyrochlore and gamma polymorphs during epitaxial stabilization, provided the proper substrate is used, opens the door for future synthesis of more compounds in complex structures *via* CSE. We also focus on demonstrating that complete structural characterization can be carried out on complex phases using CSE, demonstrating for $Sm_2Ti_2O_7$ that films are consistent with the monoclinic 110-LP and that film–substrate interfaces are smooth and the microcrystalline substrates used in CSE can be treated as local single-crystal substrates.

2 Experimental

Dense sintered substrates and targets were prepared using standard ceramic methods from commercially available (Alfa Aesar, Ward Hill, MA, all >99%) reagents of $SrCO_3$, Nb_2O_5, RE_2O_3, and TiO_2. $Sr_2Nb_2O_7$ powders (values given in parentheses are respectively for $(Dy,Gd,Sm)_2Ti_2O_7$ and $La_2Ti_2O_7$) were prepared by mixing stoichiometric quantities of the precursors, manually grinding them, and annealing them at 1400 °C (900/1200 °C and 900 °C) for 100 h (12/24 h and 12 h). Powders were reground between all annealing steps and uniaxially compacted under 150 MPa to form cylindrical pellets with a diameter of 11 mm (25.4 mm) and a thickness of 1 mm (10 mm). Pellets were annealed in air at 1400 °C (1350 °C and 1400 °C) for 100 h (24 h and 36 h). Final pellets were confirmed to be single phase using X-ray diffraction.[62,63] The $Sr_2Nb_2O_7$ substrates were then lapped flat using a 3 μm Al_2O_3 (Buehler, Lake Bluff, IL) aqueous solution, polished with a basic 0.02 μm colloidal silica solution (Buehler), and annealed in air at 1200 °C for 2 h.

$RE_2Ti_2O_7$ films were deposited using pulsed laser deposition (PLD) in similar conditions to those used successfully for other 110-LP phases.[10,28,32,33,58] Films were grown to a thickness ≈70 nm, determined using X-ray reflectivity and verified by cross-sectional transmission electron microscopy (TEM), at a substrate temperature of 900 °C, a laser energy density of 2 J cm^{-2}, a laser repetition rate of 1 Hz, and a dynamic oxygen environment of 1 mTorr O_2. Films were cooled to room temperature under a static oxygen pressure of 200 Torr.

Electron backscatter diffraction (EBSD) was used to locally characterize film orientations.[35,51,64] Backscatter patterns were acquired using a XL40FEG SEM (Phillips, Netherlands) with the sample tilted at 70°, an acceleration voltage of 25 kV, a working distance of 10 mm, and a spot size of 5 or 6 (under these conditions, the effective resolution of the EBSD system we used is approximately 20 nm[65]). Kikuchi patterns were manually collected in a point-by-point approach, Euler angles were recorded for each grain, and the Kikuchi patterns were indexed using in-house programs.[66] Secondary electron images were collected using a XL30 (Phillips) scanning electron microscope that was equipped with energy dispersive spectroscopy (Oxford Instruments, UK). To characterize the average structure, a Philips X'Pert (Philips Analytical, Netherlands) X-ray diffractometer (Cu Kα radiation) was operated at 45 kV and 40 mA in grazing incidence mode with a lens configuration to provide parallel optics, using a 2 × 2 mm^2 anti-scatter slit, a 0.27° soller slit, and a graphite monochromator.

Transmission electron microscopy (TEM) samples were prepared using a focused ion beam (FIB) lift-out approach in a Nova 600 (FEI, Oregon) dual-beam microscope on specific grains identified with EBSD in the same microscope. Pt was deposited as a protective layer on the sample surface. Back-to-back trenches were milled (using a Ga^+ ion beam operated at 30 kV, 5 nA), to leave a 1 μm-thick membrane between the trenches. The membrane was attached to an autoprobe

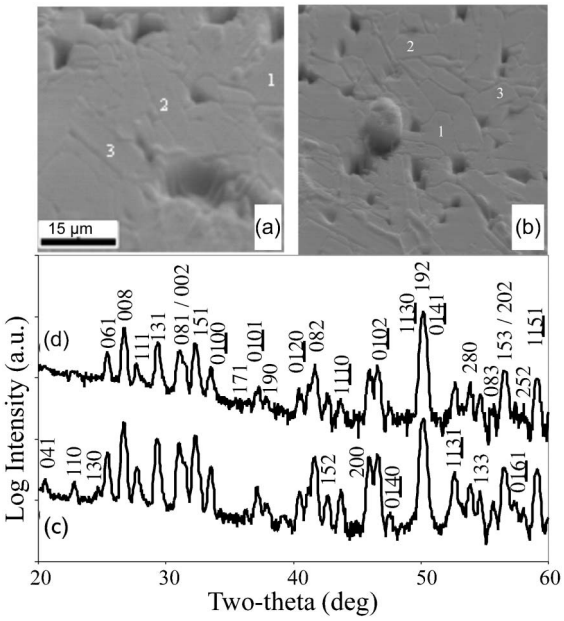

Fig. 1 Secondary electron images of (a) $Sm_2Ti_2O_7$ and (b) $Dy_2Ti_2O_7$ films on polished $Sr_2Nb_2O_7$ pellets (which exhibited identical images to these). Black regions are pores, dark lines are grain boundaries, and grey represents smooth surface features. The area for both is 50^2 μm^2. Grazing incidence X-ray diffraction patterns of (c) a bare $Sr_2Nb_2O_7$ substrate and (d) the same substrate with a $Dy_2Ti_2O_7$ film. All peaks are indexable to the substrate only, whether they are marked with their corresponding *hkl* in (c) or (d) (this is done for clarity).

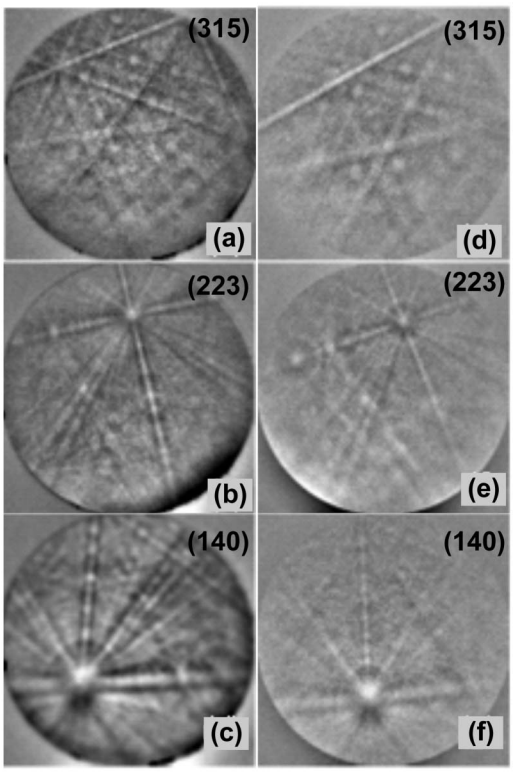

Fig. 2 Electron backscatter diffraction patterns from the $Sr_2Nb_2O_7$ substrate (a–c) and the $Sm_2Ti_2O_7$ film (d–f). In each case, the surface plane determined from the measured Euler angles is given, and these are identical (within the uncertainty) for each grain before and after film deposition. The images were registered from Grains 1 (a, d), 2 (b, e), and 3 (c, f) shown in Fig. 1(a). Substrate (film) Euler angles (°) are: grain 1 – 37 (47), 81 (86), 331 (320); grain 2 – 207 (232), 121 (130), 120 (144); grain 3 – 273 (278), 32 (37), 254 (239).

(Omniprobe, Dallas) by tungsten deposition, separated from the base using the FIB, lifted-out by the autoprobe controls, and welded onto a copper grid using Pt deposition. Finally, this 1 μm membrane was milled to electron transparency using the FIB. Selected-area electron diffraction (SAED) patterns and the corresponding high resolution electron microscopy (HREM) images were registered using an FEI Tecnai F20 field emission gun transmission electron microscope (FEGTEM) operated at 200 kV and equipped with a Gatan (Warrendale, PA) imaging filter.

3 Results and discussion

Secondary-electron SEM images of $Sm_2Ti_2O_7$ and $Dy_2Ti_2O_7$ films deposited on $Sr_2Nb_2O_7$ pellets are shown in Fig. 1(a) and 1(b), respectively. The images before deposition were indistinguishable from these. Grain boundaries and pores are clearly visible in the images, which assist in finding the same grains after deposition. Away from these boundaries, the surfaces are relatively smooth. The three grains marked in each image as 1, 2, and 3 are discussed in more detail later. EDS results supported that the $Sr_2Nb_2O_7$ substrates, which had a measured 1 : 1 Sr : Nb ratio, were uniformly covered with $RE_2Ti_2O_7$ (RE = Gd, Sm, Nd, and La) films, which had a measured composition consistent with a 1 : 1 RE : Ti ratio.

Fig. 1(c) and 1(d) respectively show the glancing angle X-ray patterns before and after deposition of a 70 nm thick $Dy_2Ti_2O_7$ film. These patterns indicate the substrate is well crystallized in the orthorhombic 110-LP structure, the indices of each diffraction peak are marked (unit cell parameters: a_o = 3.933, b_o = 26.73, c_o = 5.683 Å, where the *b*-axis is the direction of layering).[62] However, X-rays are not well suited for the identification of the film structure, as no extra peaks are observed even at the highest angles (whether peaks are marked in (c) or (d), all arise from the substrate). The absence of some peaks at low angles in (d) arises from an increased background contribution. An important point is that there is also no evidence of the stable pyrochlore phase or the kinetically preferred gamma phase in the X-ray results. The lack of additional peaks in the X-ray diffraction patterns will be shown below to arise from insufficient sensitivity of the experiment for structural characterization of these films (*i.e.*, the films are not amorphous). Similar results were observed for all $RE_2Ti_2O_7$ (RE = Dy, Gd, Sm, and La) compounds.

In Fig. 2(a–c) and 3(a–c), example EBSD patterns are given from the substrate grains marked 1–3 in Fig. 1(a) and 1(b), respectively. They are intense and have sharp contrast; all patterns observed for substrate grains were of similar quality (see ESI,† Fig. S1 and S2 for more examples). Within any individual grain, the patterns and orientation assignments

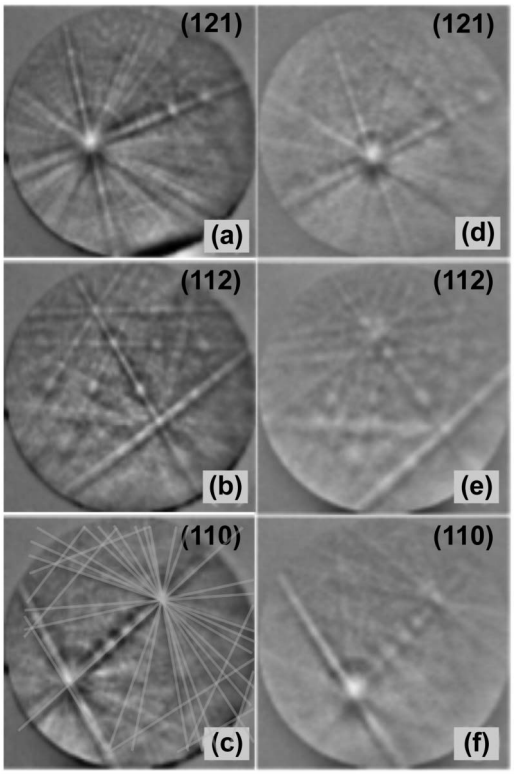

Fig. 3 Electron backscatter diffraction patterns from the $Sr_2Nb_2O_7$ substrate (a–c) and the $Dy_2Ti_2O_7$ film (d–f). In each case, the surface plane determined from the measured Euler angles is given, and these are identical (within the uncertainty) for each grain before and after film deposition. The images were registered from grains 1 (a, d), 2 (b, e), and 3 (c, f) shown in Fig. 1(b). The grey lines in (c) indicate the expected pattern from a (110) surface, indicating the reasonableness of the fit. Substrate (film) Euler angles (°) are: grain 1 – 114 (139), 141 (137), 304 (313); grain 2 – 200 (212), 66 (75), 65 (72); grain 3 – 269 (248), 116 (112), 131 (123).

were consistent. The EBSD patterns come from a depth of ≈40 nm (for the settings used), indicating that the near surface region is well crystallized and likely to support epitaxial growth. The EBSD patterns were indexed in the orthorhombic 110-LP structure by the TSL software to determine a surface plane orientation, were expressed as Miller indices, and are given in Fig. 2(a–c) and 3(a–c). The surface planes are within 5° of the indices listed. As expected, a wide orientation spread is available on the sintered pellets-ranging in just these six grains from $(110)_o$ to $(315)_o$ (and from $(001)_o$ to $(552)_o$ in the grains given in Fig. S1 and S2, ESI†). Experimental and simulated patterns, based on the software-generated orientations, were compared to confirm the assignments (one such pattern is overlayed in Fig. 3(c)). The six orientations chosen here each have a component of the orthorhombic *b*-axis in-plane, meaning the layered planes in the 110-LP structure intersect the surface plane, a surface structure that is expected to lower the kinetic barriers to growth.[10,28,32,33,58] This is in-contrast to the prior research using $SrTiO_3$ (110) single crystals,[10,32,33,58] which promote the growth of the kinetically challenged $(001)_m$-oriented films (with the layered planes parallel to the substrate surface). All $Sr_2Nb_2O_7$ substrates used herein were similar to these substrates.

Kikuchi patterns registered after deposition of ≈70 nm of $Sm_2Ti_2O_7$ and $Dy_2Ti_2O_7$ are given respectively in Fig. 2(d–f) and 3(d–f), for the same grains (1–3) whose patterns are given respectively in Fig. 2(a–c) and 3(a–c) (patterns from films of $La_2Ti_2O_7$ and $Gd_2Ti_2O_7$ are given in Fig. S1 and S2, ESI,† respectively). In all cases, film patterns are similar to the substrate patterns, but have less distinct contrast than the substrate. Relative to the substrate patterns, the film Kikuchi patterns can be rotated owing to remounting or to local misorientations related to misfit accommodation mechanisms,[67–71] and could be slightly different owing to the monoclinic structure known for the titanates.[13,53,54,56,62,72] (Since the films are shown below to be monoclinic and relaxed, some of the local misorientation is related to the latter two effects.) The important point is that the similarity of the Kikuchi patterns from the films and substrates indicate that the films grew epitaxially, in a grain-by-grain fashion.

Two important points should be made about the film EBSD data. First, scanning the beam within a grain yielded the same pattern within any grain, a pattern that changed only on traversing the grain boundaries, supporting the idea that each grain acts as a microscopic single crystal supporting epitaxial growth. Second, the bulk stable pyrochlore phase (for RE = Dy, Gd, and Sm) is easily identifiable using EBSD (based on control experiments not shown) and was not observed in any of the grains that were characterized (which included many more than the six discussed), indicating that the metastable 110-LP phase formed uniformly in these films.

The film orientations (determined relative to the *o*-$Sr_2Nb_2O_7$ structure) are given in Fig. 2(d–f) and 3(d–f); the films have identical orientations to the substrates for these six grain-orientations. Identical observations were made on $La_2Ti_2O_7$ and $Gd_2Ti_2O_7$ (Fig. S1 and S2, ESI†), as well as on many more grain orientations (not shown) for all four compositions studied. In fact, we did not find any orientations on which an epitaxial phase did not grow: in other words, we did not find any orientations where the patterns were not identical to the underlying substrate grain. These results indicate that the surfaces of polished ceramic pellets promote complex epitaxy of metastable phases and that EBSD is an effective local probe for structural characterization, reinforcing our prior observations on simpler polymorphic structures.[35,51]

$La_2Ti_2O_7$ is stable in the 110-LP structure in the bulk. While its formation as a film here is not surprising, the fact that it grows over all observed orientation space is important. It illustrates that film growth of the stable compounds can overcome kinetic barriers to their formation, which was not always the case on commercial single-crystal substrates. On the other hand, the stable bulk polymorph of $RE_2Ti_2O_7$ for RE = Gd, Sm, and Dy compositions is pyrochlore. RE = Gd, Sm compositions have been stabilized in the 110-LP thin film in earlier work on commercial $SrTiO_3$ (110) crystals.[58] On the other hand, $Dy_2Ti_2O_7$ has not been reported to adopt the 110-LP structure, neither as a thin film nor as a bulk crystal or

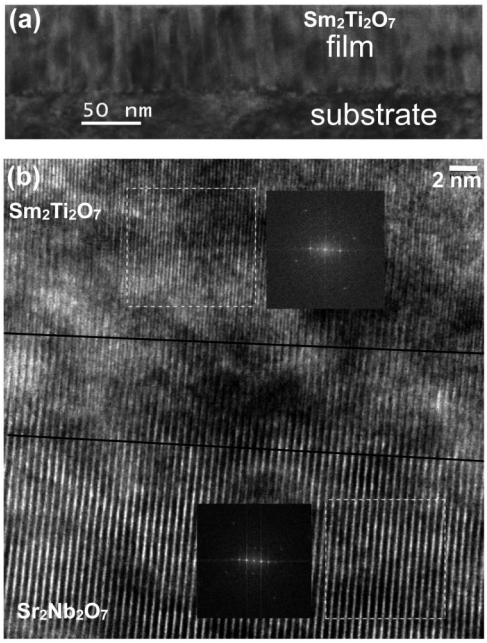

Fig. 4 TEM images taken from a cross section of grain 3 shown in Fig. 1(a). (a) A low resolution bright field image containing the $Sm_2Ti_2O_7$ film and $Sr_2Nb_2O_7$ substrate. (b) A high-resolution image focused on the film–substrate interface. The black, nearly-horizontal lines bracket the location of the interface. The insets in (b) gives the FFTs taken from the adjacent region indicated by the dashed boxes.

powder. Using CSE on a sintered $Sr_2Nb_2O_7$ substrate, we have demonstrated the facile preparation of 110-LP $Dy_2Ti_2O_7$ for a large range of surface orientations. Based on the difficulty in preparing many of these metastable phases in bulk form and as films on commercial single-crystal substrates,[10,32,33,58–61] CSE proves to be a robust method for fabricating complex materials. Future work will focus on investigating the detailed structure and property results of this new form of $Dy_2Ti_2O_7$ and other small rare-earth highly-metastable $RE_2Ti_2O_7$ films. Here, we stay focused on demonstrating the utility of the CSE technique for $Sm_2Ti_2O_7$, which only recently was shown to form in a monoclinic structure as a thin film on single crystal substrates.[58,73,74] We confirm this observation for the CSE deposited metastable compound and investigate the nature of the $Sm_2Ti_2O_2/Sr_2Nb_2O_7$ interfaces.

While EBSD provides information from $\approx$40 nm near the film surface, TEM can provide information through the thickness of the film, and specifically at the substrate-film interface. A cross-sectional TEM specimen was prepared from grain 3 marked in Fig. 1(a), whose EBSD patterns were given in Fig. 2(c) and 2(f). A low-resolution bright field TEM image is given in Fig. 4(a). The film growth appears columnar on this grain, indicated by vertical contrast. Otherwise, the films contrast is largely uniform and there is no indication of growth differences through the thickness of the 70 nm film. The interface is easily distinguished at this magnification, since the vertical contrast related to the columns terminates at the interface. Such columnar growth is often observed in the growth of complex structures on single crystal substrates.

A HREM image of this $Sm_2Ti_2O_7/Sr_2Nb_2O_7$ interface is shown in Fig. 4(b). The $Sr_2Nb_2O_7$ contrast is sharp and clear, with vertical stripes of alternating dark and light contrast. The spacing between the lines is consistent with the planes belonging to the $00l_o$ family (c_o = 5.683 Å), such that the in-plane direction (normal to them) is $<001>_o$. This is consistent with the EBSD assignment of the surface plane for this grain as $(140)_o$. The film contrast in the HREM image is less sharp, but the direction of alternating dark and light contrast is maintained across the interface region. Overall, the film appears to have a clear epitaxial arrangement with the substrate. The similarity in the fast Fourier transforms (FFTs) across the interface further confirms this assertion (the actual SAEDs are discussed further below). The approximate location of the interface is bracketed by the black guide lines, though it should be noted that the interface is not normal to the image plane, it is inclined at a small angle. Far from the interface, the vertical contrast in the film runs in the same direction as that in the substrate, though the frequency is twice that of the substrate. In general, such contrast variation can arise from changes in the imaging conditions and/or the film quality and/or symmetry differences. This image reinforces the idea that, in CSE, each microcrystalline grain at the polished surface of the sintered ceramic substrate acts as a local single crystal sample, on which metastable films can be synthesized by epitaxial stabilization. (Another HREM image from a different grain is shown in Fig. S3, ESI,† confirming these observations.)

SAED patterns, registered from the same cross section of the $Sm_2Ti_2O_7$ film described above, are given in Fig. 5. The SAED patterns are identical to the FFTs given in Fig. 4. The substrate pattern (given in Fig. 5(a)), can be indexed as the $(510)_o$ zone of the orthorhombic (o) 110-LP structure, having the $[001]_o$ in the plane of the substrate. This also agrees with the analysis of the HREM image. The SAED pattern registered from both the film and substrate is given in Fig. 5(b). The substrate grains are slightly sharper and, owing to the larger

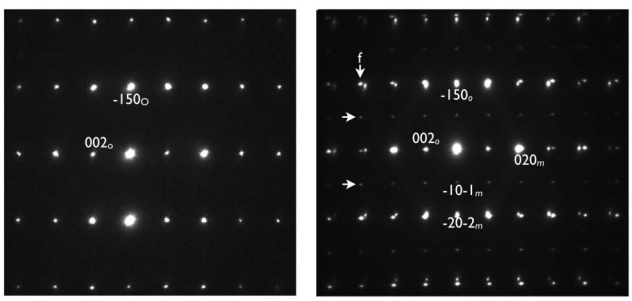

Fig. 5 SAED patterns from a cross section of $Sm_2Ti_2O_7$ grain 3 in Fig. 1(a): (a) substrate only and (b) film (f) + substrate (s). The indices with o (m) subscripts correspond to the substrate (film). Arrows point to film peaks in (b) to highlight both the smaller lattice parameter of the film in the plane of the substrate (along 002_o) and the extra rows in the direction normal to the substrate that indicate the film adopts a monoclinic structure.

lattice parameters, have a smaller repeat length in the SAED pattern. That the film peaks along the nominally in-plane direction are discernable from the substrate peaks further supports the 70 nm films are relaxed (see vertical arrow). The horizontal arrows in Fig. 5(b) highlight rows of diffraction spots that belong only to the film, indicating a difference in structure for the film compared to the substrate. These extra rows can be understood if the film is monoclinic (m), as expected from prior bulk and film studies, and the pattern can be indexed as the $(101)_m$ zone.[72] The $(101)_m$ and $(510)_o$ zones are equivalents between the two related structures, affording the high-quality epitaxy (though this may contribute to the columnar growth), and the extra rows of diffraction spots are expected in *m*-$Sm_2Ti_2O_7$. The ratio of the repeat period of the film to the substrate along these two directions are 1.056 ($010^*_m/001^*_o$) and 1.035 ($101^*_m/150^*_o$). These repeat periods of 5.38 Å and 3.06 Å for the film are reasonable for a film of $Sm_2Ti_2O_7$ (ref. 58) on $Sr_2Nb_2O_7$.[62] Observations made on other grains from the $Sm_2Ti_2O_7$ films all support the epitaxial registry between the film grains and the substrate grains (another example of a HREM image of the $Sm_2Ti_2O_7$ film on $Sr_2Nb_2O_7$ is given in Fig. S3, ESI†). All observed SAED patterns were consistent with a 110-LP $Sm_2Ti_2O_7$ film growing on all orientations of $Sr_2Nb_2O_7$.

The CSE method was previously used to investigate the nature of heterostructural epitaxy, moving away from low-index high-symmetry single crystal substrates to high-index general surfaces on polycrystals. TiO_2 films were deposited on $BaTiO_3$ (ref. 51) and $BiFeO_3$ (ref. 35) sintered ceramics. The (metastable) anatase polymorph was epitaxially grown on (001) perovskite surfaces rotated as much as 35° from the (001) surface, indicating that even high index surfaces can stabilize metastable polymorphs. In those cases, the two competing polymorphs had relatively simple structures (anatase and rutile), but neither was isostructural to the perovskite structured substrates. Nevertheless, both rutile and anatase polymorphs on perovskite substrates were, regardless of the interface plane, essentially described by a single orientation relationship with the substrate that aligned the close packed networks in three dimensions. Using CSE, it was demonstrated that heterostructural epitaxial relationships in eutactic networks may be described with a more general and simple model than two-dimensional structural matching. The current observations indicate that the CSE synthetic methodology (high-throughput characterization of a single composition grown on a polycrystalline substrate) also allows for crystal engineering in structural families that pose kinetic and thermodynamic challenges to other bulk and thin film synthetic methods. In this case, using an isostructural sintered ceramic substrate leads to the formation of a preferred coherent interface with a metastable polymorph relative to the competing pyrochlore or gamma-phase polymorphs.

The observations made here effectively represent analogous observations to thousands of publications describing epitaxial growth of both stable and metastable materials on single-crystal commercially available substrates. One area where similar observations are already well-known is in the growth of metastable layers in commercial hard coatings, where compounds such as cubic AlN are formed in metastable structures in polycrystalline superlattices.[34,75] Instead of using X-ray diffraction in combination with selective TEM, CSE uses EBSD in combination with selective TEM. With the advances in nanotechnology and local structure–property mapping over the last few decades, thin films on micron-sized crystals can be probed locally in analogous fashions to centimeter-sized crystals.

4 Conclusions

These results demonstrate that complex layered metastable compounds that could not be synthesized on commercially available substrates or as bulk powders can be synthesized on polycrystalline isostructural substrates and can be characterized locally using EBSD in a high-throughput method we call combinatorial substrate epitaxy. This opens a new avenue for thin film research where novel metastable materials, specifically shown here for $Dy_2Ti_2O_7$ in the 110-LP structure, can be synthesized using epitaxial stabilization, expanding our abilities to explore new composition–process–structure–property relationships.

Acknowledgements

The work was supported by National Science foundation grants DMR 1206656 (AMS, GSR) and CHE-0434567 (SH, KRB, PAS). Facilities supported by MRSEC program of the National Science Foundation under Award Number DMR-0520425 were used.

References

1 B. Mercey, P. A. Salvador, W. Prellier, T.-D. Doan, J. Wolfman, J.-F. Hamet, M. Hervieu and B. Raveau, *J. Mater. Chem.*, 1999, **9**, 233–242.
2 O. Y. Gorbenko, S. V. Samoilenkov, I. E. Graboy and A. R. Kaul, *Chem. Mater.*, 2002, **14**, 4026–4043.
3 D. G. Schlom, L.-Q. Chen, X. Pan, A. Schmehl and M. A. Zurbuchen, *J. Am. Ceram. Soc.*, 2008, **91**, 2429–2454.
4 S. A. Chambers, *Adv. Mater.*, 2010, **22**, 219–248.
5 P. Salvador, T. Doan, B. Mercey and B. Raveau, *Chem. Mater.*, 1998, **10**, 2592–2595.
6 G. Catalan, R. M. Bowman and J. M. Gregg, *J. Appl. Phys.*, 2000, **87**, 606–608.
7 E. Ohshima, Y. Saya, M. Nantoh and M. Kawai, *Solid State Commun.*, 2000, **116**, 73–76.
8 D. H. Kim, H. N. Lee, M. Varela and H. M. Christen, *Appl. Phys. Lett.*, 2006, **89**, 162904.
9 F. Conchon, A. Boulle, C. Girardot, S. Pignard, R. Guinebretiere, E. Dooryhee, J.-L. Hodeau, F. Weiss, J. Kreisel and J.-F. Berar, *J. Phys. D: Appl. Phys.*, 2007, **40**, 4872–4876.

10 S. Havelia, S. Wang, K. R. Balasubramaniam and P. A. Salvador, *Cryst. Growth Des.*, 2009, **9**, 4546–4554.
11 P. A. Salvador, T. O. Mason, M. E. Hagerman and K. R. Poeppelmeier, *Chemistry of Advanced Materials: An Overview*, ed. L. V. Interrante and M. Hampden-Smith, Wiley-VCH, Inc., 1998, pp. 449–498.
12 I. B. Sharma and D. Singh, *Bull. Mater. Sci.*, 1998, **21**, 363–374.
13 F. Lichtenberg, A. Herrnberger and K. Wiedenmann, *Prog. Solid State Chem.*, 2008, **36**, 253–387.
14 P. A. Salvador, B. Mercey, O. Perez, A. M. Haghiri-Gosnet, T. D. Doan and B. Raveau, *Mater. Res. Soc. Symp. Proc.*, 2000, **587**, O3.3:1–6.
15 D. Dijkkamp, T. Venkatesan, X. D. Wu, S. A. Shaheen, N. Jisrawi, Y. H. Minlee, W. L. McLean and M. Croft, *Appl. Phys. Lett.*, 1987, **51**, 619–621.
16 T. Venkatesan, C. C. Chang, D. Dijkkamp, S. B. Ogale, E. W. Chase, L. A. Farrow, D. M. Hwang, P. F. Miceli, S. A. Schwarz, J. M. Tarascon, X. D. Wu and A. Inam, *J. Appl. Phys.*, 1988, **63**, 4591–4598.
17 K. Char, D. K. Fork, T. H. Geballe, S. S. Laderman, R. C. Taber, R. D. Jacowitz, F. Bridges, G. A. N. Connell and J. B. Boyce, *Appl. Phys. Lett.*, 1990, **56**, 785–787.
18 J. S. Horwitz, D. B. Chrisey, K. S. Grabowski and R. E. Leuchtner, *Surf. Coat. Technol.*, 1992, **51**, 290–298.
19 Y. Suzuki, D. Lew, A. F. Marshall, M. R. Beasley and T. H. Geballe, *Phys. Rev. B: Condens. Matter*, 1993, **48**, 10642–10645.
20 C. Belouet, *Appl. Surf. Sci.*, 1996, **96–98**, 630–642.
21 H. Y. Zhai, I. Rusakova, R. Fairhurst and W. K. Chu, *IEEE Trans. Appl. Supercond.*, 2001, **11**, 3461–3464.
22 A. A. Bosak, C. Dubourdieu, J. P. Senateur, O. Y. Gorbenko and A. R. Kaul, *J. Mater. Chem.*, 2002, **12**, 800–801.
23 A. A. Bossak, I. E. Graboy, O. Y. Gorbenko, A. R. Kaul, M. S. Kartavtseva, V. L. Svetchnikov and H. W. Zandbergen, *Chem. Mater.*, 2004, **16**, 1751–1755.
24 K. Balasubramanian, A. Bagal, O. Castillo, A. J. Francis and P. A. Salvador, *Ceram. Trans.*, 2005, **162**, 59–68.
25 J. H. Lee, P. Murugavel, H. Ryu, D. Lee, J. Y. Jo, J. W. Kim, H. J. Kim, K. H. Kim, Y. Jo, M. H. Jung, Y. H. Oh, Y. W. Kim, J. G. Yoon, J. S. Chung and T. W. Noh, *Adv. Mater.*, 2006, **18**, 3125–3129.
26 K. R. Balasubramaniam, *PhD thesis*, Carnegie Mellon University, 2006.
27 D. Lee, J. H. Lee, P. Murugavel, S. Y. Jang, T. W. Noh, Y. Jo, M. H. Jung, Y.-D. Ko and J. S. Chung, *Appl. Phys. Lett.*, 2007, **90**, 182504.
28 K. R. Balasubramaniam, S. Havelia, P. A. Salvador, H. Zheng and J. F. Mitchell, *Appl. Phys. Lett.*, 2007, **91**, 232901.
29 V. D. Kushkov, A. V. Zverlin, A. M. Zaslavskii, A. E. Slivinskaya and A. V. Melnikov, *J. Mater. Sci.*, 1993, **28**, 361–363.
30 J. Fompeyrine, J. W. Seo and J. P. Locquet, *J. Eur. Ceram. Soc.*, 1999, **19**, 1493–1496.
31 A. Ohtomo, D. A. Muller, J. L. Grazul and H. Y. Hwang, *Appl. Phys. Lett.*, 2002, **80**, 3922–3924.
32 S. Havelia, K. R. Balasubramaniam, S. Spurgeon, F. Cormack and P. A. Salvador, *J. Cryst. Growth*, 2008, **310**, 1985–1990.
33 K. R. Balasubramaniam, Y. Cao, N. Patel, S. Havelia, P. J. Cox, E. C. Devlin, E. P. Yu, B. J. Close, P. M. Woodward and P. A. Salvador, *J. Solid State Chem.*, 2008, **181**, 705–714.
34 *Handbook of Hard Coatings*, ed. R. F. Bunshah, William Andrew Publishing/Noyes, 2001.
35 Y. Zhang, A. M. Schultz, L. Li, H. Chien, P. A. Salvador and G. S. Rohrer, *Acta Mater.*, 2012, **60**, 6486–6493.
36 H. M. Christen, S. D. Silliman and K. S. Harshavardhan, *Rev. Sci. Instrum.*, 2001, **72**, 2673–2678.
37 G. Palumbo, E. M. Lehockey and P. Lin, *JOM*, 1998, **50**, 40–43.
38 A. J. Schwartz, M. Kumar and B. L. Adams, *Electron Backscatter Diffraction in Materials Science*, Kluwer Academic Pub, 2000.
39 G. S. Rohrer, D. M. Saylor, B. El Dasher, B. L. Adams, A. D. Rollett and P. Wynblatt, *Z. Metallkd.*, 2004, **95**, 197–214.
40 A. D. Rollett, S.-B. Lee, R. Campman and G. S. Rohrer, *Annu. Rev. Mater. Sci.*, 2007, **37**, 627–658.
41 A. Goyal, D. P. Norton, D. M. Kroeger, D. K. Christen, M. Paranthaman, E. D. Specht, J. D. Budai, Q. He, B. Saffian, F. A. List, D. F. Lee, E. Hatfield, P. M. Martin, C. E. Klabunde, J. Mathis and C. Park, *J. Mater. Res.*, 1997, **12**, 2924–2940.
42 T. G. Woodcock, J. S. Abell and M. G. Hall, *J. Microcolumn Sep.*, 2002, **205**, 231–237.
43 K. Mirpuri, H. Wendrock, S. Menzel, K. Wetzig and J. Szpunar, *Microelectron. Eng.*, 2004, **76**, 160–166.
44 B. Yang, N. J. Park, B. I. Seo, Y. H. Oh, S. J. Kim, S. K. Hong, S. S. Lee and Y. J. Park, *Appl. Phys. Lett.*, 2005, **87**, 062902.
45 P. Sonnweber-Ribic, P. Gruber, G. Dehm and E. Arzt, *Acta Mater.*, 2006, **54**, 3863–3870.
46 K. De Keyser, C. Detavernier and R. L. Van Meirhaeghe, *Appl. Phys. Lett.*, 2007, **90**, 121920.
47 S. Curiotto, H. Chien, H. Meltzman, P. Wynblatt, G. S. Rohrer, W. D. Kaplan and D. Chatain, *Acta Mater.*, 2011, **59**, 5320–5331.
48 C. Trager-Cowan, F. Sweeney, J. Hastie, S. K. Manson-Smith, D. A. Cowan, D. McColl, A. Mohammed, K. P. O'Donnell, D. Zubia, S. D. Hersee, C. T. Foxon, I. Harrison and S. V. Novikov, *J. Microsc.*, 2002, **205**, 226–230.
49 A. Koblischka-Veneva, M. R. Koblischka, F. Mucklich, S. Murphy, Y. Zhou and I. V. Shvets, *IEEE Trans. Magn.*, 2006, **42**, 2873–2875.
50 A. Koblischka-Veneva, M. R. Koblischka, S. Murphy, S. K. Arora, F. Mucklich, U. Hartmann and I. V. Shvets, *J. Appl. Phys.*, 2008, **103**, 07E505.
51 N. V. Burbure, P. A. Salvador and G. S. Rohrer, *J. Am. Ceram. Soc.*, 2010, **93**, 2530–2533.
52 H. Teghidet, M. C. Bernard, S. Borensztajn, L. Chaal, S. Joiret and B. Saidani, *J. Cryst. Growth*, 2011, **331**, 72–77.
53 F. Lichtenberg, A. Herrnberger, K. Wiedenmann and J. Mannhart, *Prog. Solid State Chem.*, 2001, **29**, 1–70.
54 I. Levin and L. A. Bendersky, *Acta Crystallogr., Sect. B: Struct. Sci.*, 1999, **B55**, 853–866.
55 U. Balachandran and N. G. Eror, *J. Mater. Res.*, 1989, **4**, 1525–1528.
56 M. Gasperin, *Acta Crystallogr., Sect. B: Struct. Crystallogr. Cryst. Chem.*, 1975, **31**, 2129–2130.
57 L. Brixner, *Inorg. Chem.*, 1964, **3**, 1065–1067.

58 S. Havelia, S. Wang, K. R. Balasubramaniam and P. A. Salvador, *J. Solid State Chem.*, 2009, **182**, 1603–1610.
59 T. N. Bondarenko, V. N. Uvarov, S. V. Borisenko, Y. A. Teterin, V. P. Dzeganovski, A. M. Sych and Y. A. Titiv, *J. Korean Phys. Soc.*, 1998, **32**, S65–S67.
60 N. L. Henderson, J. Baek, P. S. Halasyamani and R. E. Schaak, *Chem. Mater.*, 2007, **19**, 1883–1885.
61 G. Shveikin and G. V. Bazuev, *Dokl. Akad. Nauk SSSR*, 1981, **266**, 1396–1399.
62 N. Ishizawa, F. Marumo, T. Kawamura and M. Kimura, *Acta Crystallogr., Sect. B: Struct. Crystallogr. Cryst. Chem.*, 1975, **31**, 1912–1915.
63 M. A. Subramanian, G. Aravamudan and G. V. S. Rao, *Prog. Solid State Chem.*, 1983, **15**, 55–143.
64 B. L. Adams, S. I. Wright and K. Kunze, *Metall. Trans. A*, 1993, **24A**, 819–831.
65 F. J. Humphreys, Y. Huang, I. Brough and C. Harris, *J. Microsc.*, 1999, **195**, 212–216.
66 J. B. Lowekamp, G. S. Rohrer, P. A. Morris Hotsenpiller, J. D. Bolt and W. E. Farneth, *J. Phys. Chem. B*, 1998, **102**, 7323–7327.
67 J. W. Matthews and A. E. Blakeslee, *J. Cryst. Growth*, 1974, **27**, 118–125.
68 J. W. Matthews and A. E. Blakeslee, *J. Cryst. Growth*, 1975, **29**, 273–280.
69 J. H. Van Der Merwe, *Philos. Mag. A*, 1982, **45**, 127–143.
70 M. Aindow and R. C. Pond, *Philos. Mag. A*, 1991, **63**, 667–694.
71 R. C. Pond, X. Ma, J. P. Hirth and T. E. Mitchell, *Philos. Mag.*, 2007, **87**, 5289–5307.
72 N. Ishizawa, F. Marumo, S. Iwai, M. Kimura and T. Kawamura, *AAPS PharmSciTech*, 1982, **38**, 368–372.
73 Z. Shao, S. Saitzek, A. Ferri, M. Rguiti, L. Dupont, P. Roussel and R. Desfeux, *J. Mater. Chem.*, 2012, **22**, 9806.
74 Z. Shao, S. Saitzek, P. Roussel and R. Desfeux, *J. Mater. Chem.*, 2012, **22**, 24894–24901.
75 S. A. Barnett, A. Madan, I. Kim and K. Martin, *MRS Bull.*, 2003, **28**, 169–172.